

E 201 162

2

**AD-A256 665**

PL-TR-92-2164



**CONTINUOUS SEISMIC THRESHOLD MONITORING**

**Frode Ringdal  
Tormod Kvaerna**

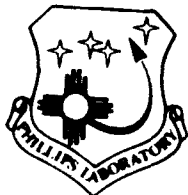
**NTNF/NORSAR  
Post Box 51  
N-2007 Kjeller, NORWAY**

31 May 1992

**DTIC  
SELECTE  
AUG 13 1992  
S D**

**Scientific Report No. 13**

**APPROVED FOR PUBLIC RELEASE; DISTRIBUTION UNLIMITED**



**PHILLIPS LABORATORY  
AIR FORCE SYSTEMS COMMAND  
HANSCOM AIR FORCE BASE, MASSACHUSETTS 01731-5000**

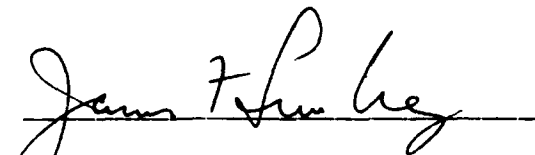
**92-22511**



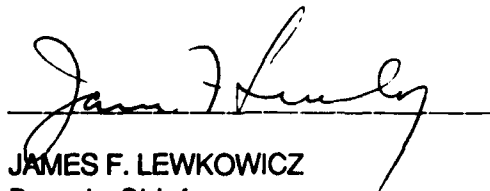
92 8 10 034

The views and conclusions contained in this document are those of the authors and should not be interpreted as representing the official policies, either expressed or implied, of the Air Force or the U.S. Government.

This technical report has been reviewed and is approved for publication.



JAMES F. LEWKOWICZ  
Contract Manager  
Solid Earth Geophysics Branch  
Earth Sciences Division



JAMES F. LEWKOWICZ  
Branch Chief  
Solid Earth Geophysics Branch  
Earth Sciences Division



DONALD H. ECKHARDT, Director  
Earth Sciences Division

This document has been reviewed by the ESD Public Affairs Office (PA) and is releasable to the National Technical Information Service (NTIS).

Qualified requestors may obtain additional copies from the Defense Technical Information Center. All others should apply to the National Technical Information Service.

If your address has changed, or if you wish to be removed from the mailing list, or if the addressee is no longer employed by your organization, please notify PL/IMA, Hanscom AFB MA 01731-5000. This will assist us in maintaining a current mailing list.

Do not return copies of this report unless contractual obligations or notices on a specific document requires that it be returned.

# REPORT DOCUMENTATION PAGE

Form Approved  
OMB No. 0704-0188

Public reporting burden for this collection of information is estimated to average 1 hour per response, including the time for reviewing instructions, searching existing data sources, gathering and maintaining the data needed, and completing and reviewing the collection of information. Send comments regarding this burden estimate or any other aspect of this collection of information, including suggestions for reducing this burden, to Washington Headquarters Services, Directorate for Information Operations and Reports, 1215 Jefferson Davis Highway, Suite 1204, Arlington, VA 22202-4302, and to the Office of Management and Budget, Paperwork Reduction Project (0704-0188), Washington, DC 20503.

<b>1. AGENCY USE ONLY (Leave blank)</b>	<b>2. REPORT DATE</b> 31 May 1992	<b>3. REPORT TYPE AND DATES COVERED</b> Scientific Report No. 13
---	--------------------------------------	---

<b>4. TITLE AND SUBTITLE</b> Continuous Seismic Threshold Monitoring	<b>5. FUNDING NUMBERS</b> PE 62714E PR 9A10 TA DA WU BH
---	---

<b>6. AUTHOR(S)</b> Frode Ringdal Tormod Kvaerna	Contract F49620-89-C-0038
--	---------------------------

<b>7. PERFORMING ORGANIZATION NAME(S) AND ADDRESS(ES)</b> NTNF/NORSAR Post Box 51 N-2007 Kjeller, NORWAY	<b>8. PERFORMING ORGANIZATION REPORT NUMBER</b>
---	---

<b>9. SPONSORING/MONITORING AGENCY NAME(S) AND ADDRESS(ES)</b> Phillips Laboratory Hanscom AFB, MA 01731-5000	<b>10. SPONSORING/MONITORING AGENCY REPORT NUMBER</b>  PL-TR-92-2164
---	--

Contract Manager: James Lewkowicz/GPEH

**11. SUPPLEMENTARY NOTES**

<b>12a. DISTRIBUTION / AVAILABILITY STATEMENT</b> Approved for public release; distribution unlimited	<b>12b. DISTRIBUTION CODE</b>
--	-------------------------------

**13. ABSTRACT (Maximum 200 words)**

Continuous threshold monitoring is a technique for using a seismic network to monitor a geographical area continuously in time. The method provides, at a given confidence level, a continuous assessment of the upper magnitude limit of possible seismic events that might have occurred in the target area. Two approaches are presented in this paper.

*Site-specific threshold monitoring:* By "focusing" a seismic network on a specific target site, continuous threshold monitoring of that site is achieved. We optimize the monitoring capability by tuning the frequency filters and array beams to known characteristics from previously recorded events at the site. We define the *threshold trace* for the network as the continuous time trace of computed upper magnitude limits of seismic events in the target area, at a 90% confidence level. As an example, we have conducted a one-week monitoring experiment of the northern Novaya Zemlya nuclear test site, using the Fennoscandian

<b>14. SUBJECT TERMS</b> Seismic monitoring Regional arrays Earthquakes	Nuclear explosions Seismic magnitudes Attenuation Network capability	<b>15. NUMBER OF PAGES</b> 30
		<b>16. PRICE CODE</b>

<b>17. SECURITY CLASSIFICATION OF REPORT</b> Unclassified	<b>18. SECURITY CLASSIFICATION OF THIS PAGE</b> Unclassified	<b>19. SECURITY CLASSIFICATION OF ABSTRACT</b> Unclassified	<b>20. LIMITATION OF ABSTRACT</b> SAR
--	---	--	--

regional array network (NORESS, ARCESS, FINESA). We find that the threshold trace is below  $m_b = 2.5$  more than 99% of the time. Thirty-four peaks exceed  $m_b = 2.5$ . All of these peaks correspond to seismic events that have been independently located by a teleseismic or regional network. During the entire one-week time period, the threshold trace exceeded  $m_b = 2.5$  only for 43 minutes.

*Regional threshold monitoring:* This involves conducting site-specific monitoring of a dense grid of geographical aiming points and requires the development of generic phase attenuation relationships for covering an extended geographical region. Using again the Fennoscandian regional array network, we illustrate the regional threshold monitoring approach by maps with color contour displays. We demonstrate that the network thresholds in Fennoscandia and adjacent regions show strong regional dependence. The thresholds are below  $m_b = 0.5$  close to each array ( $< 300$  km distance) and range from  $m_b = 2.0$  to 2.5 in parts of the Norwegian Sea and Barents Sea. The thresholds also vary significantly under different background noise conditions, and an increase of about 1.0  $m_b$  units is observed during a large teleseismic earthquake. These regional threshold maps have advantages over standard network capability maps in being more accurate during time intervals when interfering seismic events occur. They can also more easily reflect special conditions such as particularly favorable source-station propagation paths, and have the advantage of not being tied to specific event detection criteria.

The paper concludes that continuous threshold monitoring offers a valuable supplement to traditional seismic techniques used in nuclear test ban monitoring. The method may also be useful for monitoring earthquake activity at low magnitudes for sites of special interest, as well as for monitoring earthquake aftershock sequences.

## Preface

Under contract No. F49620-C-89-0038, NTNF/NORSAR is conducting research within a wide range of subjects relevant to seismic monitoring. The emphasis of the research program is on developing and assessing methods for processing of data recorded by networks of small-aperture arrays and 3-component stations, for events both at regional and teleseismic distances. In addition, more general seismological research topics are addressed.

Each quarterly technical report under this contract presents one or several separate investigations addressing specific problems within the scope of the statement of work. Summaries of the research efforts within the program as a whole are given in annual technical reports.

This Scientific Report No. 13 presents a manuscript entitled "Continuous seismic threshold monitoring", by F. Ringdal and T. Kværna.

NORSAR Contribution No. 456

DTIC QUALITY INSPECTED 8

<b>Accession For</b>	
NTIS GRA&I	<input checked="" type="checkbox"/>
DTIC TAB	<input type="checkbox"/>
Unannounced	<input type="checkbox"/>
Justification	
By _____	
Distribution/	
Availability Codes	
Dist	Avail and/or Special
A-1	

## 1 Introduction

Traditionally, seismic monitoring of earthquakes and underground explosions has relied upon applying signal detectors to individual stations within a monitoring network, associating detected phases and locating possible events in the region of interest. It is implicitly understood that such a network will have a detection threshold that varies with time. However, with methods being used in practical operation today, no attempt is made to specify this threshold as a function of time. During time periods when the background noise level is abnormally high, the event detection capabilities of such a network may be severely degraded. It is important to retain such information along with the information on the detected events.

In practice, the event detection procedure is often supplemented by assessments of network capabilities for the target region, using statistical models for the noise and signal distributions. These models include station corrections for signal attenuation and a combinatorial procedure to determine the detection threshold as a function of the number of phase detections required for reliable location (Sykes and Evernden, 1982; Harjes, 1984; Hannon, 1985; Ringdal, 1986; Sereno and Bratt, 1989).

The noise models used in these capability assessments are not able to accommodate the effect of interfering signals, such as the coda of large earthquakes, which may cause the estimated thresholds to be quite unrealistic at times. Furthermore, only a statistical capability assessment is achieved, and no indication is given as to particular time intervals when the possibility of undetected seismic events is particularly high.

The continuous threshold monitoring technique has been developed to address these problems. The basic principles were described by Ringdal and Kværna (1989), who showed that this method could be useful as a supplement to event detection analysis. In this paper we expand further on the utility of this method for site-specific seismic monitoring. In particular, we present an application in monitoring the northern Novaya Zemlya nuclear testing site using the network of advanced regional seismic arrays in Fennoscandia. A generalization of the site-specific application to a regional threshold monitoring concept is also introduced.

## 2 Method

### *Threshold monitoring -- General description*

Let us assume that we consider a network of seismic stations ( $i=1,2,\dots,N$ ) and a number of seismic phases ( $j=1,2,\dots,M$ ). For a seismic event of magnitude  $m_b=m$  an estimate  $\hat{m}_{ij}$  of  $m$  is given by

$$\hat{m}_{ij} = \log S_{ij} + b_j(\Delta, h) \quad (1)$$

where  $S_{ij}$  is the measured signal power of the  $j$ -th phase at the  $i$ -th station

$b_j(\Delta, h)$  is a distance-depth correction factor for the  $j$ -th phase.

In standard formulas for magnitude, the signal power  $S_{ij}$  is usually estimated as  $A/T$ , i.e., amplitude divided by dominant signal period.

In our case, we will assume that  $S_{ij}$  is the measurement of signal power (e.g., short term average, STA) at the expected signal arrival time. The value is measured on a single channel or array beam filtered in an appropriate frequency band.

The relation (1) is defined only for the time window corresponding to an actual seismic event. We will now consider the righthand side of (1) as a continuous function of time. Define the "threshold parameter"  $a_{ij}(t)$  as follows:

$$a_{ij}(t) = \log S_{ij}(t) + b_j(\Delta, h) \quad (2)$$

The equation (2) represents a function which can be considered as a continuous representation of the upper magnitude limit for a hypothetical seismic event at a given geographical location (target region). It coincides with the event magnitude estimate if an event occurs at that site. The function is, by definition, tied to a specific station and a specific phase.

Using a statistical approach, and assuming statistical independence of the observations, we can now proceed as described by Ringdal and Kværna (1989). We obtain a network-based representation of the upper magnitude limit by considering the function

$$g(m, t) = 1 - \prod_{i,j} \left( 1 - \Phi \left( \frac{(m - a_{ij}(t))}{\sigma_j} \right) \right) \quad (3)$$

where  $m$  is event magnitude,  $\sigma_j$  is the standard deviation of the assumed magnitude distribution for the  $j$ -th phase and  $\Phi$  denotes the standard (0,1) normal distribution function. An illustration of (3) is shown in Fig. 1.

The function  $g(m, t)$  is the probability that a given (hypothetical) seismic event of magnitude  $m$  at time  $t$  would generate signals that exceed the observed noise values at at least one station of the network. For a given  $t$ , the function  $g(m, t)$  is a monotonously increasing function of  $m$ , with values between 0 and 1.

Following Ringdal and Kværna (1989), a 90% upper limit at time  $t$  is defined as the solution to the equation

$$g(m, t) = 0.90 \quad (4)$$

The solution is a function of  $t$ , which we will denote  $m_{T90}(t)$ . We call this the *threshold trace* for the network and target region being considered.

### *Site-specific threshold monitoring*

Let us first consider threshold monitoring of a specific target area of limited geographical extent. The size of the target area may vary depending upon the application, but typically the area might be a few tens of kilometers in diameter. A basic assumption is that the target area is defined such that all seismic events within the area show similar wave propagation characteristics.

The distance-depth correction factors  $b_j(\Delta, h)$  in (1) and (2) can either be determined by using “generic” values representative for a larger region, or by calibration to the specific target area. The latter method is the most accurate and is preferable, assuming that previous calibration events are available. We then obtain the necessary magnitude calibration factors from processing previous events with known magnitude, using the relation

$$\hat{b}_{i,j} = \hat{m}_j - \log(\hat{S}_{i,j}) \quad (i = 1, \dots, K; j = 1, \dots, L) \quad (5)$$

where  $\hat{b}_{i,j}$  is our estimate of the magnitude correction factor for phase  $i$  and event  $j$ ,  $\hat{m}_j$  is the estimate of the magnitude for event  $j$  (based on independent network observations), and  $\hat{S}_{i,j}$  is our estimate of the signal level at the predicted arrival time of phase  $i$  for event  $j$ .  $K$  is the number of phases considered (there might be several stations and several phases per station), and  $L$  is the number of events.

The magnitude correction factor to be used for phase  $i$  is then given by

$$b_i = \frac{1}{L} \cdot \sum_{j=1}^L \hat{b}_{i,j} \quad (6)$$

Parameters such as window lengths for signal level estimation, travel-times of the different phases, filter frequency bands and steering delays for array beamforming are obtained on the basis of processing results for the calibration events.

### *Regional threshold monitoring*

In principle, threshold monitoring of an extended geographical region can be achieved by conducting site-specific monitoring of a dense grid of target points within that region. The density of the grid and the interpolation technique applied will determine the quality of the results.

The regional approach requires access to magnitude calibration statistics for each target point and each station/phase combination considered. In a practical situation it will usually be impossible to obtain the necessary number of calibration events for each target point in the grid, and a different approach is therefore required.

Our approach is to develop a “generic” attenuation model for the region to be monitored. This can be done as a two-step process. The first step is to divide the region into



subareas that are relatively homogeneous with respect to wave propagation characteristics. Within each subarea, an attenuation model is then established on the basis of available calibration data.

Using this approach, the distance-depth correction factors  $b_j(\Delta, h)$  in (1) and (2) can be determined individually for each seismic phase, by applying standard least-squares techniques. In this paper we have used the results of Alsaker et al (1991) and Kværna (1991).

In threshold monitoring there is a tradeoff between the size of the target area and the tolerances of the parameter values used in the threshold computations. With a given grid, it is necessary to make the target area of each aiming point compatible with the grid spacing.

An illustration of the time and azimuth tolerances is given in Figs. 2 and 3. For example, if we increase the time windows over which we measure the signal levels  $\hat{S}_{i,j}$  in (5), this has the effect of broadening the target area for the aiming point. At the same time, some of the resolution in the regional threshold variation will be lost. A similar consideration applies if we increase the allowable azimuth tolerances. For a more detailed discussion of this problem, reference is made to Kværna (1991).

### 3 Site-specific threshold monitoring

#### *Application to the Novaya Zemlya test site*

In order to demonstrate how site-specific threshold monitoring could be performed in a practical operational situation, we have conducted an experiment during which we have applied continuous threshold monitoring to the northern Novaya Zemlya test site (Lilwall and Marshall, 1986) for a full one-week period. Our data base has been the Fennoscandian regional array network (NORESS, ARCESS, FINESA). As illustrated in Fig. 4, these three arrays are all within regional distances from the test site.

The excellent P-phase detection capabilities of these arrays are illustrated in Fig. 5, which shows recorded P waves from the 24 October 1990 nuclear explosion at Novaya Zemlya ( $m_b = 5.7$ ). A simple scaling of the noise traces as shown in the figure indicates that ARCESS would have detected even an event three orders of magnitude smaller (i.e., about magnitude 2.7). NORESS and FINESA have somewhat lower capabilities for this target area. The ARCESS array also detects S phases from Novaya Zemlya explosions quite well, whereas NORESS and FINESA have a lower S-phase detection capability.

The parameters used in the threshold monitoring experiment are given in Table 1. For each array, we steer "optimum" P and S beams towards the test site, and calibrate these beams using actually observed signal attenuation from available Novaya Zemlya explosion recordings. By focusing in this way on the target region, we can at any point in time measure the "noise magnitude" for a given phase at a given array, and combine these data to obtain a network threshold as previously explained.

For the Novaya Zemlya test site, only large explosions have been available to calibrate the three arrays. The effect of a spectral shift at lower magnitudes is uncertain. We have selected the "optimum" filters with a sufficient bandwidth to accommodate the expected range of dominant frequencies from  $m_b = 2.5$  to 5.5. These frequencies have been estimated based on recorded data from chemical explosions and earthquakes at various distance ranges.

## Results

Figs. 6 and 7 show results from two days of the monitoring experiment. Each of the figures covers one data day. The upper three traces of each figure represent the thresholds (i.e., 90% upper magnitude limits) obtained from the three individual arrays, whereas the bottom trace illustrates the network threshold. Typically, the individual array traces have a number of significant peaks for each 24-hour period, due to interfering events (local or teleseismic). On the network trace, the number and sizes of these peaks are greatly reduced, because an interfering event will usually not provide matching signals at all the stations. From probabilistic considerations, it can in such cases be inferred that the actual network threshold is lower than these individual peaks might indicate. Fig. 8 shows the cumulative statistics of the network thresholds for the full one-week period.

On each of the one-day figures, we have included comments explaining the presence of the most significant peaks on the network trace. The number of peaks and the total time exceeding given magnitude thresholds are summarized in Fig. 9. Here, we will just note that the first day, 24 October 1990, was the day of the previously mentioned nuclear explosion ( $m_b = 5.7$ ) on Novaya Zemlya, and this event naturally stands out on the plot. While the peak value of the network threshold plot does not represent the actual magnitude of the event, it is in fact quite close (5.64).

As a general comment to Figs. 6 and 7, we note that such plots enable the analyst to obtain an instant assessment of the actual threshold level of the monitoring network. The peaks on the network traces may be quickly correlated with a detection bulletin, in order to decide whether they originate from interfering events or from events in the target region. At NORSAR, such detection information is currently provided by the Intelligent Monitoring System (Bache et al, 1990).

The advantage of the threshold monitoring approach is that, for a given target site and at a specified threshold level for events of interest, only a very few peaks would need to be examined. For example, experience from monitoring Novaya Zemlya shows that there are many days with no significant peak at all, and the number of peaks above  $m_b = 2.5$  seldom exceeds 3 or 4 during a day.

## 4 Regional threshold monitoring

### *Application to Fennoscandia and adjacent regions*

As previously discussed, regional threshold monitoring is an extension of the original site-specific threshold monitoring concept. It entails using the same basic principles to obtain wide geographical coverage, including coverage of regions for which no calibration events are available. The key to achieving this is to develop generic relations for attenuation and magnitude corrections of seismic phases of interest, and to deploy a sufficient number of beams to ensure adequate geographical coverage.

Kværna (1991) has developed initial such generic relations for the Pn and Lg phases of NORESS, ARCESS and FINESA using the method outlined previously. The relations are applicable to northern Europe and adjacent regions, and are based on a systematic analysis of several hundred phase observations of regional events in various geographical areas. These results form the basis for the study presented in this section.

### *Threshold maps*

The regional threshold monitoring approach lends itself naturally to displays in the form of contoured geographical maps. By using a spatial grid covering the area of interest, interpolation can be applied to get a visual representation of threshold variations over an extended geographical region.

Using the generic relations developed by Kværna (1991), we computed a threshold monitoring grid of 20 x 30 geographical aiming points (see Fig. 10) for two 40-minute time intervals. Data from the three arrays NORESS, ARCESS and FINESA were used. Contouring maps were developed by interpolation in this grid, and displayed in the form of color maps where the color scale is tied to the actual threshold.

Fig. 11 and 12 show two representative examples of output from this procedure.

Fig. 11 illustrates *absolute* TM threshold levels (with  $m_b$  units indicated on the color template). The top part shows the absolute threshold levels at a specific time during a typically "quiet" period (i.e., no seismic event occurring). We note that the areas immediately surrounding each array (blue or green) show the lowest thresholds (below  $m_b = 0.5$ ), whereas most of the remaining area at regional distances has a yellow color, indicating thresholds in the range  $m_b = 0.5-1.5$ . The orange color seen further away from the network stations indicates thresholds of  $m_b$  1.5 to 2.0.

The bottom part of Fig. 11 shows the absolute threshold levels during "interfering event" conditions, i.e., a few minutes after the arrival of P waves from a large distant earthquake (South of Kermadec Islands,  $m_b = 5.4$ ). The threshold level has been raised by approximately one magnitude unit over the entire Fennoscandian region, although the increase is not uniform. In fact, the exact picture will change continuously with time as the P wavefront and the P coda waves move across the area.

Fig. 12 illustrates *relative* TM threshold levels. By *relative* thresholds we mean thresholds relative to the long-term average for each geographical aiming point. The top part of Fig. 12 shows the levels at a typical "quiet" period, and the various shades of blue indicate that no activity apart from normal noise fluctuations are occurring.

The bottom part of Fig. 12 shows a typical *relative* map at a time corresponding to a mining explosion (magnitude  $m_L = 2.2$ ) near Kirovsk ( $67.6^\circ\text{N}$ ,  $34.0^\circ\text{E}$ ) in the Kola Peninsula. The purpose of displaying *relative* thresholds is to emphasize more clearly the effects of the seismic event in causing threshold increases both within and outside the source area. We note that, naturally, the area surrounding the mining site has the highest relative threshold (red), whereas "side lobe" effects cause significant threshold increase also in other regions, some of which are quite far apart from the mine.

## 5 Discussion

The continuous threshold monitoring technique represents a new approach toward achieving reliable seismic monitoring. As discussed in this paper, the method is well suited to supplement the traditional methods in monitoring potential test sites for the purpose of verifying nuclear test ban treaties. The method may equally well be used to monitor earthquake activity at low magnitudes for sites of special interest, and could also be useful for monitoring earthquake aftershock sequences. We have demonstrated how the concept can be used to enable threshold monitoring of extended geographical regions, with possible applications to real-time displays.

It is important to be aware that the main purpose of the threshold monitoring method is to call attention to any time instance when a given threshold is exceeded. This will enable the analyst to focus his efforts on those events that are truly of interest in a monitoring situation. He will then apply other, traditional analysis tools in detecting, locating and characterizing the source of the disturbance. Thus, the threshold monitoring method is a supplement to, and not a replacement of, traditional methods.

### *Site-specific threshold monitoring*

It is significant that the 3-array network studied in this paper can monitor the Novaya Zemlya test site down to  $m_b$  2.5 or below more than 99% of the time (Fig. 8). Further improvements would clearly be possible by adding more stations to the monitoring network, especially highly sensitive stations at other azimuths than those covered by the Fennoscandian arrays. This would in particular contribute to lowering the peaks due to interfering events, whereas any event truly originating in the target region would still stand out clearly on the combined network traces.

In a nuclear test ban monitoring situation, it will be important to isolate and analyze more extensively those time intervals which offer significant evasion opportunities. Fig. 9 gives a statistic of the number of occasions during which the upper magnitude limit exceeded a given level for the one-week monitoring experiment. In theory, if this limit is,

e.g., at 3.0, it might be possible that a clandestine  $m_b = 3.0$  explosion had occurred without being detected. There are many options available to investigate such a hypothesis in more detail, although we have not attempted to do so in this study. The most immediate approach would be to analyze high-frequency signals for the time interval being considered. For example, on ARCESS records Novaya Zemlya explosions will contain significant energy at 10 Hz and above, even at magnitudes well below 3.0. Teleseismic events, even of large  $m_b$ , will contain relatively less energy at these frequencies and thus it might be possible to obtain additional indications from these data.

To assess interfering phases from events at regional distances is more difficult, since the high-frequency energy might not discriminate such events from Novaya Zemlya explosions. In such cases, additional procedures, such as maximum likelihood beamforming, might become useful to suppress signals from the interfering event and thereby obtain a more realistic estimate of the signal energy arriving from the target region.

### *Regional threshold monitoring*

The regional threshold maps are in some ways similar to the standard network capability maps traditionally used in seismic monitoring studies (Network, Snap/D, etc.). Especially Fig. 11, which gives "absolute" thresholds, could be seen as a capability map. However, there are some fundamental differences:

- Standard capability maps use as a basis statistical models of signal and noise characteristics; in particular a signal variance and a noise variance is assumed to compensate for statistical fluctuations. In contrast, the regional TM maps give "snapshots" of the capability as actually observed at a given point in time.
- With standard maps, no allowance is made for unusual conditions, such as, e.g., the occurrence of a large earthquake or an aftershock sequence which may cause the network capability to deteriorate for hours. With the TM approach, the actual variation in detection capability is immediately apparent.
- Standard capability maps require assumptions, e.g., with regard to "SNR threshold required for detection" and "minimum number of stations required to locate". The TM maps require no such assumptions since they are not tied to "detecting and locating" seismic events, but rather describe directly the observed "seismic field" at any point in time.

We will briefly comment further on the last item mentioned above: The requirement of multistation detection with the standard method will sometimes result in unrealistically high thresholds, e.g., in areas near a station of the monitoring network. The multistation requirement also implies that the method is not able to adequately represent the possibility of particularly favorable source-station paths. A case in point is the outstanding capability of the NORESS array in detecting explosions at Semipalatinsk (Ringdal, 1990). Thus, if NORESS has no detection, it is highly unlikely that any explosion at that site of  $m_b > 3$  has occurred, whereas a capability map based on a 4-station detection requirement may well show a threshold an order of magnitude higher.

The threshold monitoring approach will avoid these inconsistencies. Thus, under normal noise conditions, the thresholds will be very low within a few hundred km of each network station. Furthermore, since the TM thresholds are dominated by the "best" station of the network, particularly favorable source/receiver paths may be accommodated, although this would require a combination of regional and site-specific monitoring.

In conclusion, the continuous threshold monitoring has been demonstrated to provide a simple and very effective tool in day-to-day monitoring of a site of particular interest. Further research will focus upon developing methods to analyze time intervals during which significant evasion possibilities might exist. Data from the regional arrays, the large-aperture NORSAR array, as well as other available stations, will be used in these analyses.

### *Acknowledgement*

This research is sponsored by Advanced Research Projects Agency of the U.S. Department of Defense, through the Air Force Geophysics Laboratory, under contract no. F49610-89-C-0038. The prototype regional threshold monitoring display which forms the basis for the color illustrations in this paper has been developed Rolf M. Aasen of NORSAR, using the "NOGRA" graphics software system.

### *References*

- Alsaker, A., L.B. Kvamme, R.A. Hansen, A. Dahle and H. Bungum (1991): The  $M_L$  scale in Norway, *Bull. Seism. Soc. Am.*, Vol 81, 379-398.
- Bache, T.C., S.R. Bratt, J. Wang, R.M. Fung, C. Kobryn and J.W. Given (1990): The Intelligent Monitoring System, *Bull. Seism. Soc. Am.*, Vol 80, Special Issue, 1833-1851.
- Fyen, J. (1986): NORESS noise spectral studies -- Beam suppression, *Sci. Rep. 1-86/87*, NTNF/, NORSAR, Kjeller, Norway.
- Hannon, W. (1985): Seismic verification of a comprehensive test ban, *Science* 227, 251-257.
- Harjes, H.-P. (1984): Global seismic network assessment for teleseismic detection of underground nuclear explosions, *Tech. Rep. C84-02*, Center for Seismic Studies, Washington, D.C.
- Kværna, T. and F. Ringdal (1990): Continuous threshold monitoring of the Novaya Zemlya test site, *Semiannual Tech. Summary*, 1 Apr - 30 Sep 1990, NORSAR *Sci. Rep. 1-90/91*, NORSAR, Kjeller, Norway.

- 
- Kværna, T. (1991): Initial development of generic relations for regional threshold monitoring, Semiannual Tech. Summary, 1 Oct 1990 - 31 Mar 91, NORSAR Sci. Rep. 2-90/91, NORSAR, Kjeller, Norway.
- Lilwall, R.C. and P.D. Marshall (1986): Body wave magnitudes and locations of Soviet underground explosions at the Novaya Zemlya test site, AWRE Rep. NO. 017/86.
- Ringdal, F. and T. Kværna (1989): A multichannel processing approach to real time network detection, phase association and threshold monitoring, Bull. Seism. Soc. Am., Vol 79, 1927-1940.
- Ringdal, F. (1986): Study of magnitudes, seismicity and earthquake detectability using a global network, Bull. Seism. Soc. Am., Vol 76, 1641-1659.
- Ringdal, F. (1990): Teleseismic event detection using the NORESS array, with special reference to low-yield Semipalatinsk Explosions, Bull. Seism. Soc. Am., Vol 80, Special Issue, 2127-2142.
- Ringdal, F. and T. Kværna (1990): Continuous threshold monitoring using "regional threshold displays", Semiannual Tech. Summary, 1 Oct 1990 - 31 Mar 91, NORSAR Sci. Rep. 2-90/91, NORSAR, Kjeller, Norway.
- Sereno, T.J. and S.R. Bratt (1989): Seismic detection capability at NORESS and implications for the detection threshold of a hypothetical network in the Soviet Union, J. Geophys. Res., 94, B8, 10397-10414.
- Sykes, L. and J. Evernden (1982): The verification of a comprehensive nuclear test ban, Sci. Am., 247, 47-55.

Station	Phase	Tr.Time	App. Vel.	Azim.	Filter	Config.	STA_Len.	Tim.Tol.	STA_Calib.
ARC	Pn	148.0	9.9	60.5	3.0-5.0	A0,B,C,D	2.0	2.0	0.754
ARC	Sn	257.0	4.9	53.2	3.0-5.0	A0,B,C,D	5.0	3.0	1.176
FIN	P	228.0	9.6	32.9	2.0-4.0	A0,B,C	2.0	2.0	1.520
NRS	P	284.0	10.4	28.1	1.5-3.5	A0,B,C,D	2.0	2.0	0.677

Tr.Time	--	Travel time of phase
App. Vel.	--	Apparent velocity from broadband F-K measurements
Azim.	--	Azimuth from broadband F-K measurement
Filter	--	Cutoffs of bandpass filter (3rd order Butterworth)
Config.	--	Array configuration used in beamforming. A0,B,C means A0Z, B-ring and C-ring
STA_Len.	--	STA length in seconds
Tim.Tol.	--	Time tolerance when searching for maximum STA
STA_Calib.	--	Calibration factor used when converting STA values (in quantum units) to magnitude Magnitude = $\log_{10}(\text{STA}) + \text{STA\_Calib.}$

**Table 1.** Parameters used for site-specific monitoring of the northern Novaya Zemlya test site.



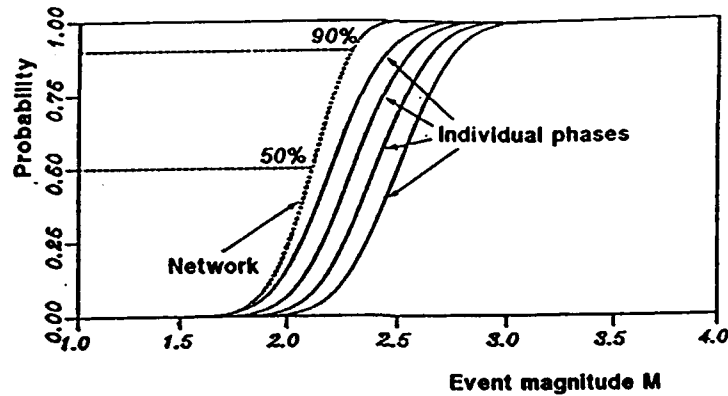


Fig. 1. Illustration of the procedure for calculating upper magnitude limits. Each seismic phase gives rise to a probability distribution, as illustrated on the figure. The dotted curve,  $g(M,t)$ , represents the probability, given event magnitude  $M$ , that the signal from a hypothetical event occurring at time  $t$  would exceed the actually observed noise level at at least one station. (After Ringdal and Kværna, 1989.)

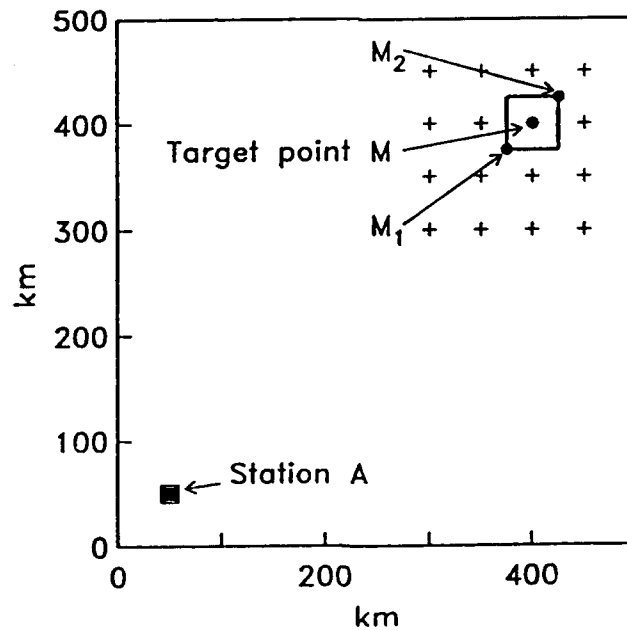


Fig. 2. This figure illustrates the necessity of using time tolerances. The plus signs indicate target points, and a rectangle surrounding one of the target points ( $M$ ) is also given. The point within the rectangle with the minimum travel time is denoted  $M_1$ , whereas the point with the maximum travel time is denoted  $M_2$ .

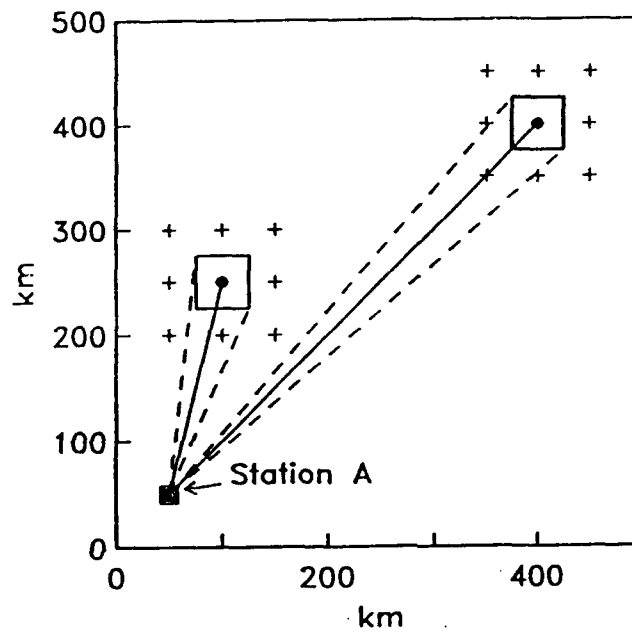


Fig. 3. In order to monitor a finite area surrounding each of the target points, a mis-steering in azimuth is introduced when the beams are steered towards the target points. This figure illustrates this for two target points at different distances. The azimuth deviations are indicated by dashed lines. Also note that for a fixed grid spacing, the mis-steering is a function of distance to the target points.

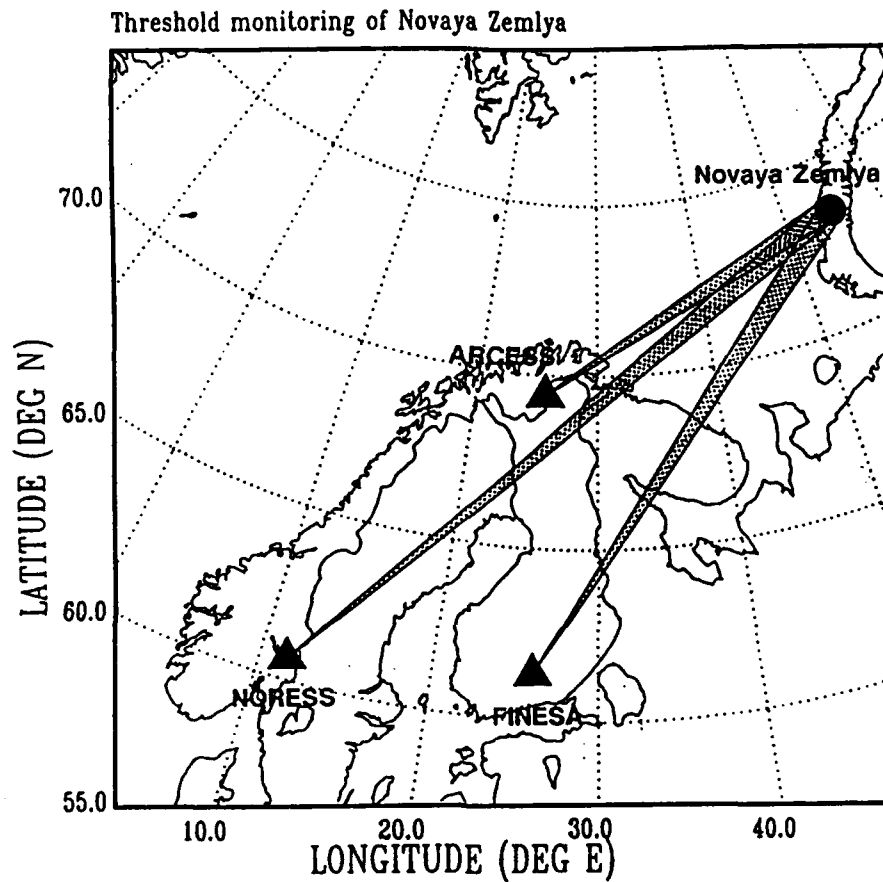


Fig. 4. Location of the target area (the northern Novaya Zemlya test site) for the threshold monitoring experiment. The locations of the three arrays NORESS ( $\Delta = 2280$  km), ARCESS ( $\Delta = 1100$  km) and FINESA ( $\Delta = 1780$  km) are indicated.

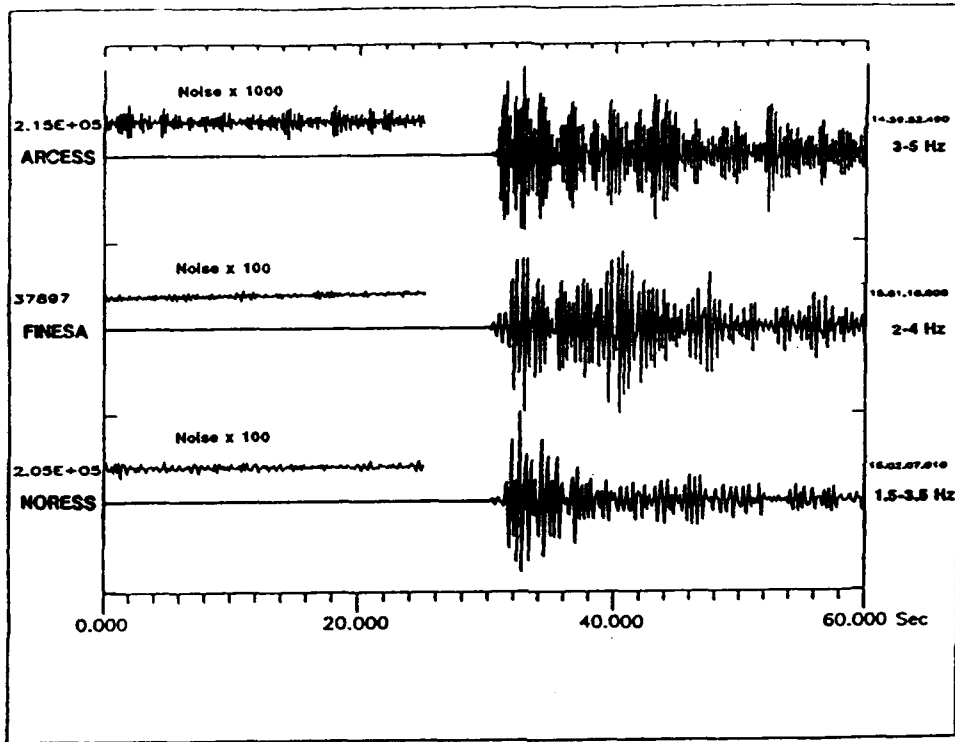


Fig. 5. P-wave recordings (filtered array beams) at ARCESS, FINESA and NORESS for the Novaya Zemlya nuclear explosion 24 October 1990. To illustrate the high signal-to-noise ratios, noise traces scaled by factors of 1000 (ARCESS) and 100 (FINESA and NORESS) are displayed for each array.

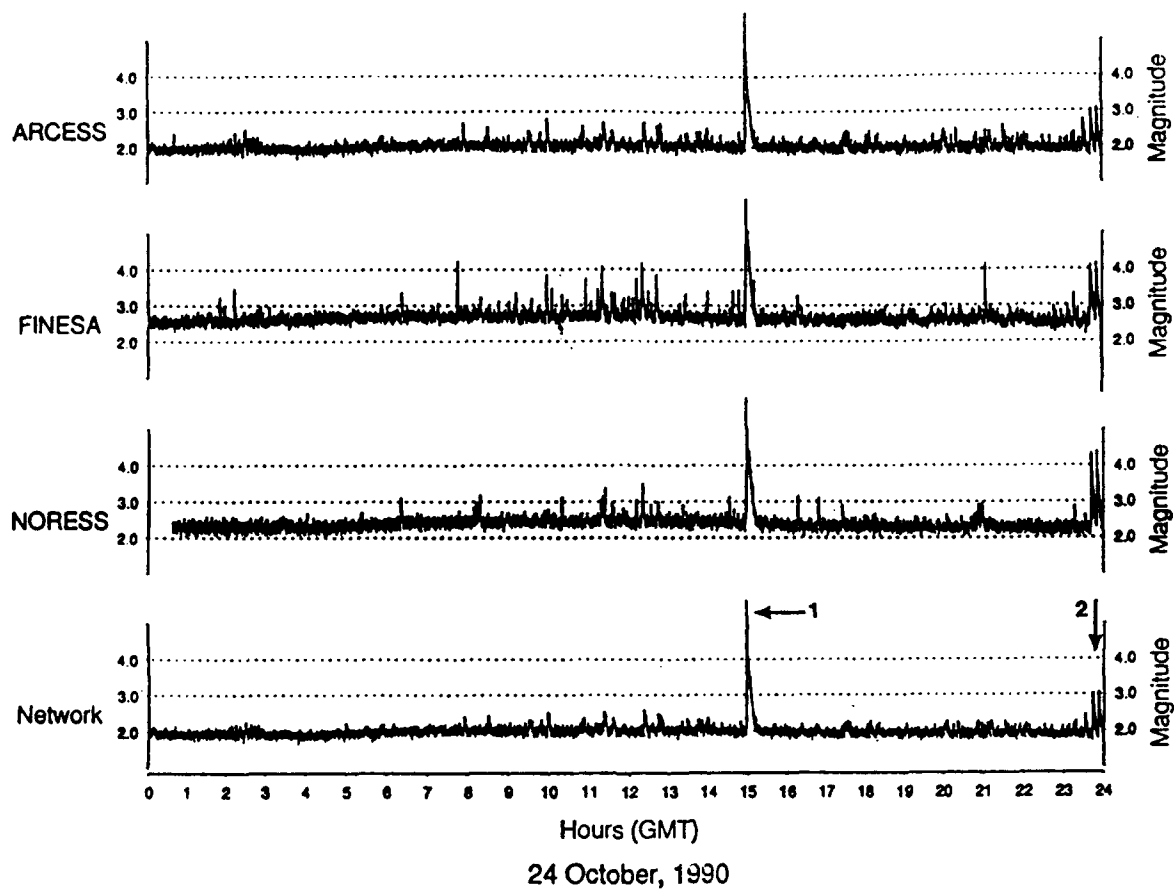


Fig. 6. Threshold monitoring of the Novaya Zemlya test site for day 297 (24 October 1990). The top three traces represent thresholds (upper 90 per cent magnitude limits) obtained from each of the three arrays (ARCESS, FINESA, NORESS), whereas the bottom trace shows the combined network thresholds.

Notes:

1. An underground nuclear explosion ( $m_b = 5.7$ ) at Novaya Zemlya at 14:58:00 GMT. The peak of the network trace is 5.64.
2. Two teleseismic earthquakes from N. Xinjang province, China ( $m_b = 5.2$  and 5.4). The P-wave and coda from each of these earthquakes cause the network threshold to increase to about  $m_b = 3.0$  for the target region.

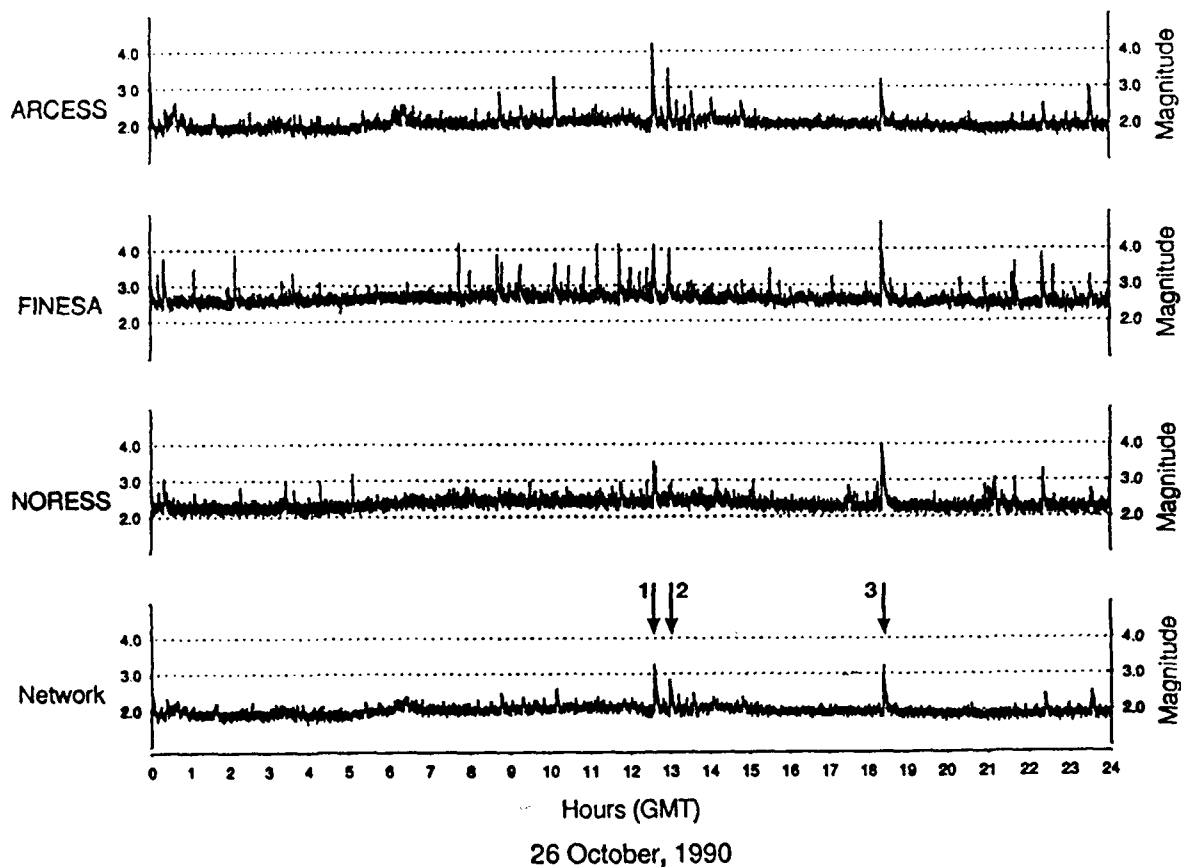


Fig. 7. Same as Fig. 6, but for day 299 (26 October 1990).

Notes:

1. A mining explosion ( $M_L = 3.0$ ) near the Norway-USSR border. The Novaya Zemlya threshold peak is  $m_b = 3.2$ . Note that this threshold exceeds the event magnitude; this is because of the proximity of the event to the network stations.
2. A mining explosion ( $M_L = 2.5$ ) at the Kola Peninsula. The network threshold peak is  $m_b = 2.8$ .
3. A teleseismic earthquake ( $m_b = 5.1$ ) near Lake Baikal. The network threshold peak is  $m_b = 3.2$ .

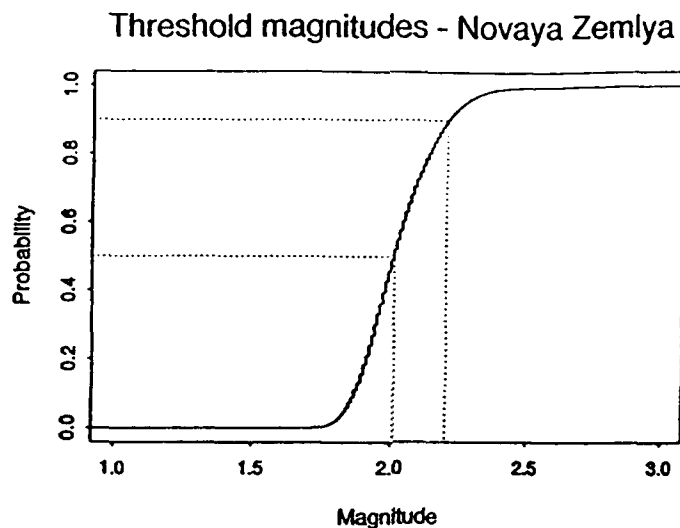


Fig. 8. Cumulative statistics of the network threshold magnitudes from one full week of data, October 24-30, 1990.

24-30 October, 1990

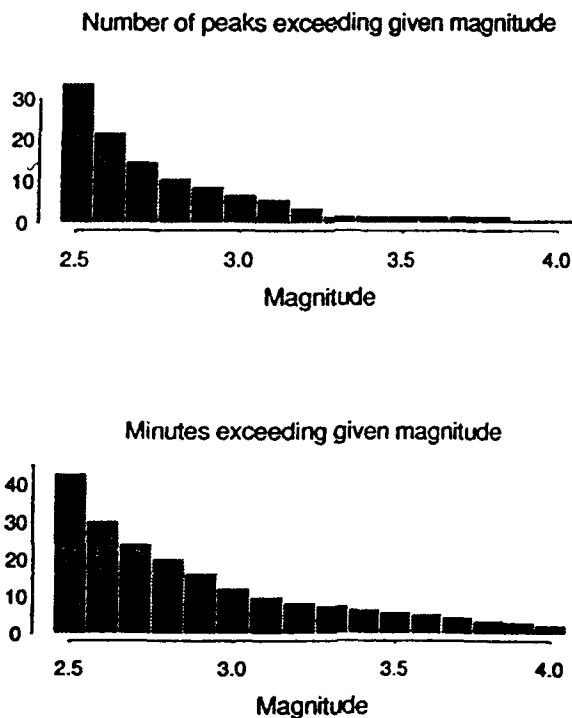


Fig. 9. Statistics of peaks in the network threshold traces for the one-week monitoring experiment of Novaya Zemlya: a) Number of peaks exceeding given  $m_b$  values and b) Total duration of peaks above  $m_b = 2.5$ .

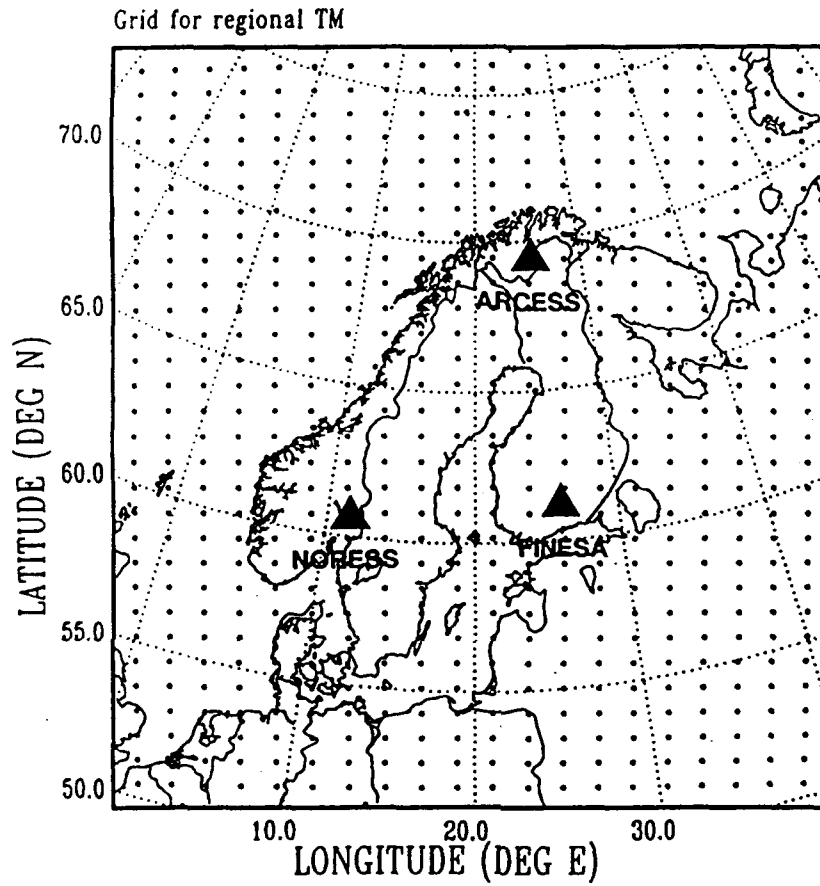


Fig. 10. Beam grid used for calculating regional thresholds with the array network NORESS, ARCESS, and FINESA. The location of the three arrays is shown on the map.



DISTRIBUTION LIST

Prof. Thomas Ahrens  
Seismological Lab, 252-21  
Division of Geological & Planetary Sciences  
California Institute of Technology  
Pasadena, CA 91125

Prof. Keiiti Aki  
Center for Earth Sciences  
University of Southern California  
University Park  
Los Angeles, CA 90089-0741

Prof. Shelton Alexander  
Geosciences Department  
403 Deike Building  
The Pennsylvania State University  
University Park, PA 16802

Dr. Ralph Alewine, III  
DARPA/NMRO  
3701 North Fairfax Drive  
Arlington, VA 22203-1714

Prof. Charles B. Archambeau  
CIRES  
University of Colorado  
Boulder, CO 80309

Dr. Thomas C. Bache, Jr.  
Science Applications Int'l Corp.  
10260 Campus Point Drive  
San Diego, CA 92121 (2 copies)

Prof. Muawia Barazangi  
Institute for the Study of the Continent  
Cornell University  
Ithaca, NY 14853

Dr. Jeff Barker  
Department of Geological Sciences  
State University of New York  
at Binghamton  
Vestal, NY 13901

Dr. Douglas R. Baumgardt  
ENSCO, Inc  
5400 Port Royal Road  
Springfield, VA 22151-2388

Dr. Susan Beck  
Department of Geosciences  
Building #77  
University of Arizona  
Tucson, AZ 85721

Dr. T.J. Bennett  
S-CUBED  
A Division of Maxwell Laboratories  
11800 Sunrise Valley Drive, Suite 1212  
Reston, VA 22091

Dr. Robert Blandford  
AFTAC/TT, Center for Seismic Studies  
1300 North 17th Street  
Suite 1450  
Arlington, VA 22209-2308

Dr. G.A. Bollinger  
Department of Geological Sciences  
Virginia Polytechnic Institute  
21044 Derring Hall  
Blacksburg, VA 24061

Dr. Stephen Bratt  
Center for Seismic Studies  
1300 North 17th Street  
Suite 1450  
Arlington, VA 22209-2308

Dr. Lawrence Burdick  
Woodward-Clyde Consultants  
566 El Dorado Street  
Pasadena, CA 91109-3245

Dr. Robert Burrige  
Schlumberger-Doll Research Center  
Old Quarry Road  
Ridgefield, CT 06877

Dr. Jerry Carter  
Center for Seismic Studies  
1300 North 17th Street  
Suite 1450  
Arlington, VA 22209-2308

Dr. Eric Chael  
Division 9241  
Sandia Laboratory  
Albuquerque, NM 87185

Prof. Vernon F. Cormier  
Department of Geology & Geophysics  
U-45, Room 207  
University of Connecticut  
Storrs, CT 06268

Prof. Steven Day  
Department of Geological Sciences  
San Diego State University  
San Diego, CA 92182

Marvin Denny  
U.S. Department of Energy  
Office of Arms Control  
Washington, DC 20585

Dr. Zoltan Der  
ENSCO, Inc.  
5400 Port Royal Road  
Springfield, VA 22151-2388

Prof. Adam Dziewonski  
Hoffman Laboratory, Harvard University  
Dept. of Earth Atmos. & Planetary Sciences  
20 Oxford Street  
Cambridge, MA 02138

Prof. John Ebel  
Department of Geology & Geophysics  
Boston College  
Chestnut Hill, MA 02167

Eric Fielding  
SNEE Hall  
INSTOC  
Cornell University  
Ithaca, NY 14853

Dr. Mark D. Fisk  
Mission Research Corporation  
735 State Street  
P.O. Drawer 719  
Santa Barbara, CA 93102

Prof Stanley Flatte  
Applied Sciences Building  
University of California, Santa Cruz  
Santa Cruz, CA 95064

Dr. John Foley  
NER-Geo Sciences  
1100 Crown Colony Drive  
Quincy, MA 02169

Prof. Donald Forsyth  
Department of Geological Sciences  
Brown University  
Providence, RI 02912

Dr. Art Franke!  
U.S. Geological Survey  
922 National Center  
Reston, VA 22092

Dr. Cliff Frolich  
Institute of Geophysics  
8701 North Mopac  
Austin, TX 78759

Dr. Holly Given  
IGPP, A-025  
Scripps Institute of Oceanography  
University of California, San Diego  
La Jolla, CA 92093

Dr. Jeffrey W. Given  
SAIC  
10260 Campus Point Drive  
San Diego, CA 92121

Dr. Dale Glover  
Defense Intelligence Agency  
ATTN: ODT-1B  
Washington, DC 20301

Dr. Indra Gupta  
Teledyne Geotech  
314 Montgomery Street  
Alexandria, VA 22314

Dan N. Hagedorn  
Pacific Northwest Laboratories  
Battelle Boulevard  
Richland, WA 99352

Dr. James Hannon  
Lawrence Livermore National Laboratory  
P.O. Box 808  
L-205  
Livermore, CA 94550

Dr. Roger Hansen  
HQ AFTAC/TTR  
Patrick AFB, FL 32925-6001

Prof. David G. Harkrider  
Seismological Laboratory  
Division of Geological & Planetary Sciences  
California Institute of Technology  
Pasadena, CA 91125

Prof. Danny Harvey  
CIRES  
University of Colorado  
Boulder, CO 80309

Prof. Donald V. Helmberger  
Seismological Laboratory  
Division of Geological & Planetary Sciences  
California Institute of Technology  
Pasadena, CA 91125

Prof. Eugene Herrin  
Institute for the Study of Earth and Man  
Geophysical Laboratory  
Southern Methodist University  
Dallas, TX 75275

Prof. Robert B. Herrmann  
Department of Earth & Atmospheric Sciences  
St. Louis University  
St. Louis, MO 63156

Prof. Lane R. Johnson  
Seismographic Station  
University of California  
Berkeley, CA 94720

Prof. Thomas H. Jordan  
Department of Earth, Atmospheric &  
Planetary Sciences  
Massachusetts Institute of Technology  
Cambridge, MA 02139

Prof. Alan Kafka  
Department of Geology & Geophysics  
Boston College  
Chestnut Hill, MA 02167

Robert C. Kemerait  
ENSCO, Inc.  
445 Pineda Court  
Melbourne, FL 32940

Dr. Max Koontz  
U.S. Dept. of Energy/DP 5  
Forrestal Building  
1000 Independence Avenue  
Washington, DC 20585

Dr. Richard LaCoss  
MIT Lincoln Laboratory, M-200B  
P.O. Box 73  
Lexington, MA 02173-0073

Dr. Fred K. Lamb  
University of Illinois at Urbana-Champaign  
Department of Physics  
1110 West Green Street  
Urbana, IL 61801

Prof. Charles A. Langston  
Geosciences Department  
403 Deike Building  
The Pennsylvania State University  
University Park, PA 16802

Jim Lawson, Chief Geophysicist  
Oklahoma Geological Survey  
Oklahoma Geophysical Observatory  
P.O. Box 8  
Leonard, OK 74043-0008

Prof. Thorne Lay  
Institute of Tectonics  
Earth Science Board  
University of California, Santa Cruz  
Santa Cruz, CA 95064

Dr. William Leith  
U.S. Geological Survey  
Mail Stop 928  
Reston, VA 22092

Mr. James F. Lewkowicz  
Phillips Laboratory/GPEH  
Hanscom AFB, MA 01731-5000( 2 copies)

Mr. Alfred Lieberman  
ACDA/VI-OA State Department Building  
Room 5726  
320-21st Street, NW  
Washington, DC 20451

Prof. L. Timothy Long  
School of Geophysical Sciences  
Georgia Institute of Technology  
Atlanta, GA 30332

Dr. Randolph Martin, III  
New England Research, Inc.  
76 Olcott Drive  
White River Junction, VT 05001

Dr. Robert Masse  
Denver Federal Building  
Box 25046, Mail Stop 967  
Denver, CO 80225

Dr. Gary McCartor  
Department of Physics  
Southern Methodist University  
Dallas, TX 75275

Prof. Thomas V. McEvelly  
Seismographic Station  
University of California  
Berkeley, CA 94720

Dr. Art McGarr  
U.S. Geological Survey  
Mail Stop 977  
U.S. Geological Survey  
Menlo Park, CA 94025

Dr. Keith L. McLaughlin  
S-CUBED  
A Division of Maxwell Laboratory  
P.O. Box 1620  
La Jolla, CA 92038-1620

Stephen Miller & Dr. Alexander Florence  
SRI International  
333 Ravenswood Avenue  
Box AF 116  
Menlo Park, CA 94025-3493

Prof. Bernard Minster  
IGPP, A-025  
Scripps Institute of Oceanography  
University of California, San Diego  
La Jolla, CA 92093

Prof. Brian J. Mitchell  
Department of Earth & Atmospheric Sciences  
St. Louis University  
St. Louis, MO 63156

Mr. Jack Murphy  
S-CUBED  
A Division of Maxwell Laboratory  
11800 Sunrise Valley Drive, Suite 1212  
Reston, VA 22091 (2 Copies)

Dr. Keith K. Nakanishi  
Lawrence Livermore National Laboratory  
L-025  
P.O. Box 808  
Livermore, CA 94550

Dr. Carl Newton  
Los Alamos National Laboratory  
P.O. Box 1663  
Mail Stop C335, Group ESS-3  
Los Alamos, NM 87545

Dr. Bao Nguyen  
HQ AFTAC/TTR  
Patrick AFB, FL 32925-6001

Prof. John A. Orcutt  
IGPP, A-025  
Scripps Institute of Oceanography  
University of California, San Diego  
La Jolla, CA 92093

Prof. Jeffrey Park  
Kline Geology Laboratory  
P.O. Box 6666  
New Haven, CT 06511-8130

Dr. Howard Patton  
Lawrence Livermore National Laboratory  
L-025  
P.O. Box 808  
Livermore, CA 94550

Dr. Frank Pilotte  
HQ AFTAC/TT  
Patrick AFB, FL 32925-6001

Dr. Jay J. Pulli  
Radix Systems, Inc.  
2 Taft Court, Suite 203  
Rockville, MD 20850

Dr. Robert Reinke  
ATTN: FCTVID  
Field Command  
Defense Nuclear Agency  
Kirtland AFB, NM 87115

Prof. Paul G. Richards  
Lamont-Doherty Geological Observatory  
of Columbia University  
Palisades, NY 10964

Mr. Wilmer Rivers  
Teledyne Geotech  
314 Montgomery Street  
Alexandria, VA 22314

Dr. George Rothe  
HQ AFTAC/TTR  
Patrick AFB, FL 32925-6001

Dr. Alan S. Ryall, Jr.  
DARPA/NMRO  
3701 North Fairfax Drive  
Arlington, VA 22209-1714

Dr. Richard Sailor  
TASC, Inc.  
55 Walkers Brook Drive  
Reading, MA 01867

Prof. Charles G. Sammis  
Center for Earth Sciences  
University of Southern California  
University Park  
Los Angeles, CA 90089-0741

Prof. Christopher H. Scholz  
Lamont-Doherty Geological Observatory  
of Columbia University  
Palisades, CA 10964

Dr. Susan Schwartz  
Institute of Tectonics  
1156 High Street  
Santa Cruz, CA 95064

Secretary of the Air Force  
(SAFRD)  
Washington, DC 20330

Office of the Secretary of Defense  
DDR&E  
Washington, DC 20330

Thomas J. Sereno, Jr.  
Science Application Int'l Corp.  
10260 Campus Point Drive  
San Diego, CA 92121

Dr. Michael Shore  
Defense Nuclear Agency/SPSS  
6801 Telegraph Road  
Alexandria, VA 22310

Dr. Matthew Sibol  
Virginia Tech  
Seismological Observatory  
4044 Derring Hall  
Blacksburg, VA 24061-0420

Prof. David G. Simpson  
IRIS, Inc.  
1616 North Fort Myer Drive  
Suite 1440  
Arlington, VA 22209

Donald L. Springer  
Lawrence Livermore National Laboratory  
L-025  
P.O. Box 808  
Livermore, CA 94550

Dr. Jeffrey Stevens  
S-CUBED  
A Division of Maxwell Laboratory  
P.O. Box 1620  
La Jolla, CA 92038-1620

Lt. Col. Jim Stobie  
ATTN: AFOSR/NL  
Bolling AFB  
Washington, DC 20332-6448

Prof. Brian Stump  
Institute for the Study of Earth & Man  
Geophysical Laboratory  
Southern Methodist University  
Dallas, TX 75275

Prof. Jeremiah Sullivan  
University of Illinois at Urbana-Champaign  
Department of Physics  
1110 West Green Street  
Urbana, IL 61801

Prof. L. Sykes  
Lamont-Doherty Geological Observatory  
of Columbia University  
Palisades, NY 10964

Dr. David Taylor  
ENSCO, Inc.  
445 Pineda Court  
Melbourne, FL 32940

Dr. Steven R. Taylor  
Los Alamos National Laboratory  
P.O. Box 1663  
Mail Stop C335  
Los Alamos, NM 87545

Prof. Clifford Thurber  
University of Wisconsin-Madison  
Department of Geology & Geophysics  
1215 West Dayton Street  
Madison, WS 53706

Prof. M. Nafi Toksoz  
Earth Resources Lab  
Massachusetts Institute of Technology  
42 Carleton Street  
Cambridge, MA 02142

Dr. Larry Turnbull  
CIA-OSWR/NED  
Washington, DC 20505

DARPA/RMO/SECURITY OFFICE  
3701 North Fairfax Drive  
Arlington, VA 22203-1714

Dr. Gregory van der Vink  
IRIS, Inc.  
1616 North Fort Myer Drive  
Suite 1440  
Arlington, VA 22209

HQ DNA  
ATTN: Technical Library  
Washington, DC 20305

Dr. Karl Veith  
EG&G  
5211 Auth Road  
Suite 240  
Suitland, MD 20746

Defense Intelligence Agency  
Directorate for Scientific & Technical Intelligence  
ATTN: DTIB  
Washington, DC 20340-6158

Prof. Terry C. Wallace  
Department of Geosciences  
Building #77  
University of Arizona  
Tuscon, AZ 85721

Defense Technical Information Center  
Cameron Station  
Alexandria, VA 22314 (2 Copies)

Dr. Thomas Weaver  
Los Alamos National Laboratory  
P.O. Box 1663  
Mail Stop C335  
Los Alamos, NM 87545

TACTEC  
Battelle Memorial Institute  
505 King Avenue  
Columbus, OH 43201 (Final Report)

Dr. William Wortman  
Mission Research Corporation  
8560 Cinderbed Road  
Suite 700  
Newington, VA 22122

Phillips Laboratory  
ATTN: XPG  
Hanscom AFB, MA 01731-5000

Prof. Francis T. Wu  
Department of Geological Sciences  
State University of New York  
at Binghamton  
Vestal, NY 13901

Phillips Laboratory  
ATTN: GPE  
Hanscom AFB, MA 01731-5000

AFTAC/CA  
(STINFO)  
Patrick AFB, FL 32925-6001

Phillips Laboratory  
ATTN: TSML  
Hanscom AFB, MA 01731-5000

DARPA/PM  
3701 North Fairfax Drive  
Arlington, VA 22203-1714

Phillips Laboratory  
ATTN: SUL  
Kirtland, NM 87117 (2 copies)

DARPA/RMO/RETRIEVAL  
3701 North Fairfax Drive  
Arlington, VA 22203-1714

Dr. Michel Bouchon  
I.R.I.G.M.-B.P. 68  
38402 St. Martin D'Herès  
Cedex, FRANCE

Dr. Michel Campillo  
Observatoire de Grenoble  
I.R.I.G.M.-B.P. 53  
38041 Grenoble, FRANCE

Dr. Jorg Schlittenhardt  
Federal Institute for Geosciences & Nat'l Res.  
Postfach 510153  
D-3000 Hannover 51, GERMANY

Dr. Kin Yip Chun  
Geophysics Division  
Physics Department  
University of Toronto  
Ontario, CANADA

Dr. Johannes Schweitzer  
Institute of Geophysics  
Ruhr University/Bochum  
P.O. Box 1102148  
4360 Bochum 1, GERMANY

Prof. Hans-Peter Harjes  
Institute for Geophysic  
Ruhr University/Bochum  
P.O. Box 102148  
4630 Bochum 1, GERMANY

Prof. Eystein Husebye  
NTNF/NORSAR  
P.O. Box 51  
N-2007 Kjeller, NORWAY

David Jepsen  
Acting Head, Nuclear Monitoring Section  
Bureau of Mineral Resources  
Geology and Geophysics  
G.P.O. Box 378, Canberra, AUSTRALIA

Ms. Eva Johannisson  
Senior Research Officer  
National Defense Research Inst.  
P.O. Box 27322  
S-102 54 Stockholm, SWEDEN

Dr. Peter Marshall  
Procurement Executive  
Ministry of Defense  
Blacknest, Brimpton  
Reading FG7-FRS, UNITED KINGDOM

Dr. Bernard Massinon, Dr. Pierre Mechler  
Societe Radiomana  
27 rue Claude Bernard  
75005 Paris, FRANCE (2 Copies)

Dr. Svein Mykkeltveit  
NTNT/NORSAR  
P.O. Box 51  
N-2007 Kjeller, NORWAY (3 Copies)

Prof. Keith Priestley  
University of Cambridge  
Bullard Labs, Dept. of Earth Sciences  
Madingley Rise, Madingley Road  
Cambridge CB3 0EZ, ENGLAND